PERGAMON

Available at
www.ElsevierComputerScience.com
POWERED BY SCIENCE DIRECT

Pattern Recognition 37 (2004) 189–199

PATTERN RECOGNITION
THE JOURNAL OF THE PATTERN RECOGNITION SOCIETY
www.elsevier.com/locate/patcog

Fuzzy clustering and enumeration of target type based on sonar returns

Billur Barshan*, Birsel Ayrulu

Department of Electrical Engineering, Bilkent University, Bilkent, TR-06800 Ankara, Turkey

Received 20 August 2002; accepted 26 June 2003

Abstract

The fuzzy *c*-means (FCM) clustering algorithm is used in conjunction with a cluster validity criterion, to determine the number of different types of targets in a given environment, based on their sonar signatures. The class of each target and its location are also determined. The method is experimentally verified using real sonar returns from targets in indoor environments. A correct differentiation rate of 98% is achieved with average absolute valued localization errors of 0.5 cm and 0.8° in range and azimuth, respectively.
© 2003 Pattern Recognition Society. Published by Elsevier Ltd. All rights reserved.

Keywords: Target classification; Target differentiation; Target localization; Fuzzy *c*-means clustering; Sonar sensing

1. Introduction

Intelligent systems, especially those which interact with or act upon their surroundings need the model of the environment in which they operate. They can obtain this model partly or entirely using one or more sensors and/or viewpoints. An important example of such systems is fully or partly autonomous mobile robots. For instance, considering typical indoor environments, a mobile robot must be able to differentiate planar walls, corners, edges, and cylinders for map-building, navigation, obstacle avoidance, and target-tracking purposes.

Reliable target differentiation is crucial for robust operation and is highly dependent on the mode(s) of sensing employed. One of the most useful and cost-effective modes of sensing for mobile robot applications is sonar sensing. The fact that acoustic sensors are light, robust and inexpensive devices has led to their widespread use in applications such as navigation of autonomous vehicles through unstructured environments [1–4], map-building [5–7], target-tracking [8], and obstacle avoidance [9]. Although there are difficulties in the interpretation of sonar data due to poor angular resolution of sonar, multiple and higher-order reflections, and establishing correspondence between multiple echoes on different receivers [10,11], these difficulties can be overcome by employing accurate physical models for the reflection of sonar.

In this paper, we investigate the determination of the number of different types of targets, in an environment containing many targets of several types, based on their sonar signatures. In addition to determining the number of types of targets, we also determine the class of each target and its location. The fact that the targets are located at different positions with respect to the observer complicates the classification problem, since identical or similar targets must be grouped in the same class despite the fact that their sonar signatures are altered as a result of their different positions. Of the many potential applications, of special interest to us is a mobile robot roaming in an environment where it encounters the various types of targets at different locations within its field of view. Alternatively, the observer might be stationary and the targets moving, or both the observer and the targets might be in motion.

Our method is based on the fuzzy *c*-means (FCM) clustering algorithm which iteratively determines the cluster

* Corresponding author. Tel.: +90-312-290-2161; fax: +90-312-266-4192.
E-mail address: billur@ee.bilkent.edu.tr (B. Barshan).

0031-3203/$30.00 © 2003 Pattern Recognition Society. Published by Elsevier Ltd. All rights reserved.
doi:10.1016/S0031-3203(03)00226-7

centers and fuzzy cluster membership values, and a cluster validity criterion balancing compactness and separation of the clusters to determine the number of different target types. We present results based on experimental data acquired with low-cost ultrasonic transducers, which will be described in detail in the next section. More concretely, an ultrasonic sensing unit transmitting and receiving ultrasonic pulses has been used to collect angular amplitude and time-of-flight (TOF) scans from unknown targets, to be processed to reveal the number of different types of targets, the class of each target, and its position. The targets we consider to illustrate our method are those commonly encountered in indoor environments, such as planes, corners, edges, and cylinders. A correct differentiation rate of 98% is achieved and the targets are localized with average absolute valued range and azimuth errors of 0.5 cm and 0.8°, respectively.

We note that the position-invariant pattern recognition and position estimation achieved in this paper is different from such operations performed on conventional images [12,13] in that here we work not on direct "photographic" images of the targets obtained by some kind of imaging system, but rather on angular sonar scans obtained by rotating a sensing unit. The targets we differentiate are not patterns in a two-dimensional image whose coordinates we try to determine, but rather objects in space, exhibiting depth, whose position with respect to the sensing system we need to estimate. As such, position-invariant differentiation and localization is achieved with an approach quite different than those employed in invariant pattern recognition and localization in conventional images. In particular, the effect of position on the sonar signatures of the targets cannot be characterized by simple operations such as scaling, shifting and rotations so that standard techniques employed in two-dimensional pattern recognition to achieve invariance to such operations are not applicable (for instance, see Refs. [14–16]). Indeed, there is no simple relationship between the signatures of the same target at different positions, making the differentiation and localization process difficult.

This paper is organized as follows: Section 2 reviews the basics of sonar sensing and describes the acquisition and the structure of the sonar data. The FCM clustering algorithm and the cluster validity criterion are summarized in Section 3. In Section 4, we outline the method used to determine the positions of the targets. Experimental results are provided in Section 5. Concluding remarks and directions for future work are given in the last section.

2. Sonar sensing and data acquisition

Sonar ranging systems commonly employ only the TOF information, recording the time elapsed between the transmission and reception of a pulse. In commonly used TOF systems, an echo is produced when the transmitted pulse encounters an object and a range measurement $r = vt_\circ/2$ is obtained when the echo amplitude is detected at the receiver at time $t_\circ$. Here, $t_\circ$ is the TOF and v is the speed of sound in air (at room temperature, $v = 343.3$ m/s). Since the standard electronics for the widely used Polaroid sensor [17] do not provide the echo amplitude directly, most sonar systems rely only on TOF information. A comparison of various TOF estimation techniques can be found in Ref. [18]. Differential TOF models of targets have been used by several researchers: In Ref. [19], a single sensor is used for map building. First, edges are differentiated from planes/corners from a single vantage point. Then, planes and corners are differentiated by scanning from two separate locations using the TOF information in the complete sonar scans of the targets. Rough surfaces have been considered in Refs. [6,20]. In Ref. [5], a similar approach has been proposed to identify these targets as beacons for mobile robot localization. A tri-aural sensor configuration which consists of one transmitter and three receivers to differentiate and localize planes, corners, and edges using only the TOF information is employed in Ref. [10]. A similar sensing configuration is used to estimate the radius of curvature of cylinders in Refs. [21,22]. Differentiation of planes, corners, and edges is extended to 3-D using three transmitter/receiver pairs (transceivers) in Refs. [23,24] where these transceivers are placed on the corners of an equilateral triangle. Manyika has used differential TOF models for target tracking [25]. Systems using only qualitative information [8], combining amplitude, energy, and duration of the echo signals together with TOF information [6,26,27], or exploiting the complete echo signal [28] have also been considered.

A major problem with using the amplitude information of sonar signals is that the amplitude is very sensitive to environmental conditions and decreases with increasing target distance from the transducer as well as with deviation from the line-of-sight. For this reason, and also because the standard electronics typically provide only TOF data, amplitude information is rarely used. We exploit the normally unexploited amplitude information by designing and using customized electronic circuitry. Barshan and Kuc's early work on the use of amplitude information [27] to differentiate planes and corners has been extended to a variety of target types in Ref. [26] using both amplitude and TOF information. In the present paper, fuzzy clustering is used to exploit both amplitude and TOF information from multiple ultrasonic transducers to improve the angular resolution and to reliably handle the target classification problem.

The major limitation of sonar sensors comes from their large beamwidth. Although these devices return accurate range data, they cannot provide direct information on the angular position of the object from which the reflection was obtained. Sensory information from a *single* sonar has poor angular resolution and is usually not sufficient to differentiate more than a small number of target primitives [27]. With a single stationary transducer, it is not possible to estimate the azimuth of a target with better resolution than $2\theta_\circ$ (Fig. 1(a)). Improved target classification can be achieved

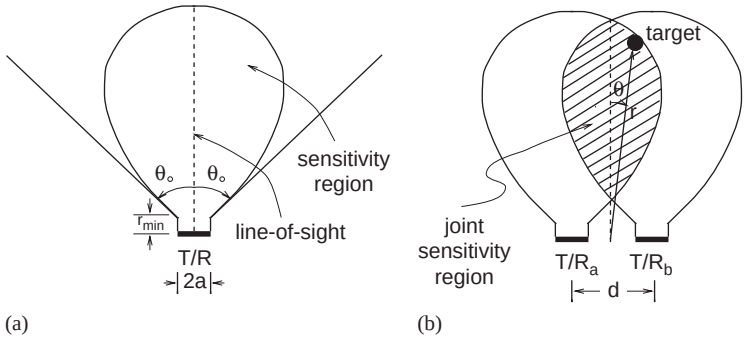

Fig. 1. (a) Sensitivity region of an ultrasonic transducer. (b) Joint sensitivity region of a pair of ultrasonic transducers. The intersection of the individual sensitivity regions serves as a reasonable approximation to the joint sensitivity region.

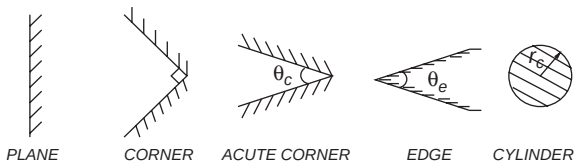

Fig. 2. Horizontal cross-sections of the targets differentiated in this study.

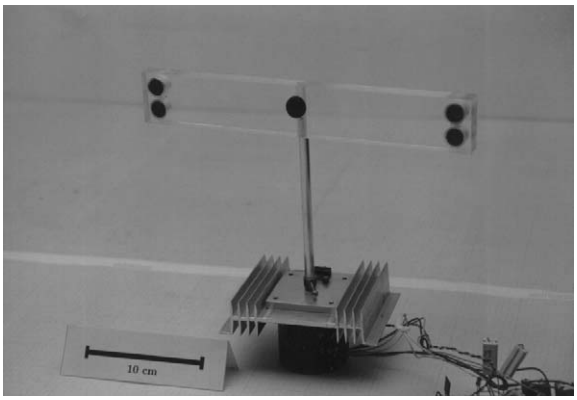

Fig. 3. Configuration of the Panasonic transducers in the real sonar system. The upper transducers are transmitters and the lower transducers are receivers. The two transducers on the left collectively constitute one transmitter/receiver, denoted T/R, and those on the right constitute another.

by using multi-transducer pulse/echo systems and by employing both amplitude and TOF information. The key for our successful use of amplitude information is the joint use of amplitude information together with TOF information from more than one sensor. While amplitude information is prone to environmental conditions, it nevertheless represents substantial extra information which, when combined with TOF information, allows considerable improvement.

A two-transducer configuration is employed in this study (Fig. 1(b)). Each transmitter–receiver pair can detect echo signals reflected from targets within its *sensitivity region* (Fig. 1(a)). Both members of the sensor configuration can detect targets located within the *joint sensitivity region* (Fig. 1(b)). The target range r and azimuth θ are defined with respect to the mid-point of the two-transducer configuration. Since the wavelength ($\lambda \cong 8.6$ mm at $f_\circ = 40$ kHz) is much larger than the typical roughness of surfaces encountered in indoor environments, targets in these environments reflect acoustic beams specularly, like a mirror.

In our experiments, we have employed targets commonly encountered in indoor environments such as *plane*, *corner*, *acute corner*, *edge*, and *cylinder* (Fig. 2). In particular, we have employed a planar target, a corner of $\theta_c = 90°$, an acute corner of $\theta_c = 60°$, an edge of $\theta_e = 90°$, and cylinders with radii $r_c = 2.5, 5.0$, and 7.5 cm, all made of wood.

Panasonic transducers [29] with aperture radius $a = 0.65$ cm, resonance frequency $f_\circ = 40$ kHz, and beamwidth $2\theta_\circ = 108°$ are used in our experiments. Since Panasonic transducers are manufactured as separate transmitting and receiving units (Fig. 3), separate transmitting and receiving elements with a small vertical spacing have been used. The horizontal center-to-center separation of the transducer units used is $d = 25$ cm. The entire sensing unit is mounted on a small 6 V computer-controlled stepper motor with step size 1.8°. The motion of the stepper motor is controlled through the parallel port of a PC486 with the aid of a microswitch. Data acquisition from the sonars is through a PC A/D card with 12-bit resolution and 1 MHz sampling frequency. Starting at the transmit time, 10,000 samples of each echo signal are collected to record the peak amplitude and the TOF.

Amplitude and TOF patterns are collected in this manner for 100 targets randomly situated in the sectoral region defined by 30 cm $\leqslant r \leqslant$ 60 cm and $-25° \leqslant \theta \leqslant 25°$. The target located at range r and azimuth θ is scanned by the rotating sensing unit for scan angles $-52° \leqslant \alpha \leqslant 52°$ with 1.8° increments (determined by the step size of the

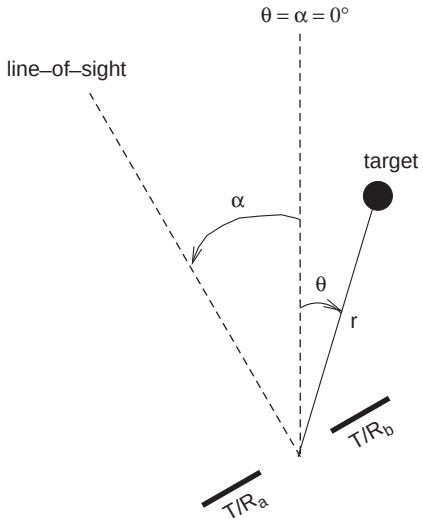

Fig. 4. Scan angle α and the target azimuth θ.

motor). The reason for using a wider range for the scan angle is the possibility that a target may still generate returns outside of the range of θ. The angle α is always measured with respect to $\theta = 0°$ regardless of target location (r, θ). (That is, $\theta = 0°$ and $\alpha = 0°$ coincide as shown in Fig. 4.)

At each step of the scan (for each value of α), four sonar echo signals are acquired. The echo signals are in the form of slightly skewed wave packets [30] (Fig. 5). In the figure, A_{aa}, A_{bb}, A_{ab}, and A_{ba} denote the peak values of the echo signals, and t_{aa}, t_{bb}, t_{ab}, and t_{ba} denote their TOF delays (extracted by simple thresholding). The first subscript indicates the transmitting transducer, the second denotes the receiver. At each step of the scan, only these eight amplitude and TOF values extracted from the four echo signals are recorded. For the given scan range and motor step size, 58 $(=2 \times 52°/1.8°)$ angular samples of each of the amplitude and TOF patterns $A_{aa}(\alpha)$, $A_{bb}(\alpha)$, $A_{ab}(\alpha)$, $A_{ba}(\alpha)$, $t_{aa}(\alpha)$, $t_{bb}(\alpha)$, $t_{ab}(\alpha)$, and $t_{ba}(\alpha)$ are acquired for each target.

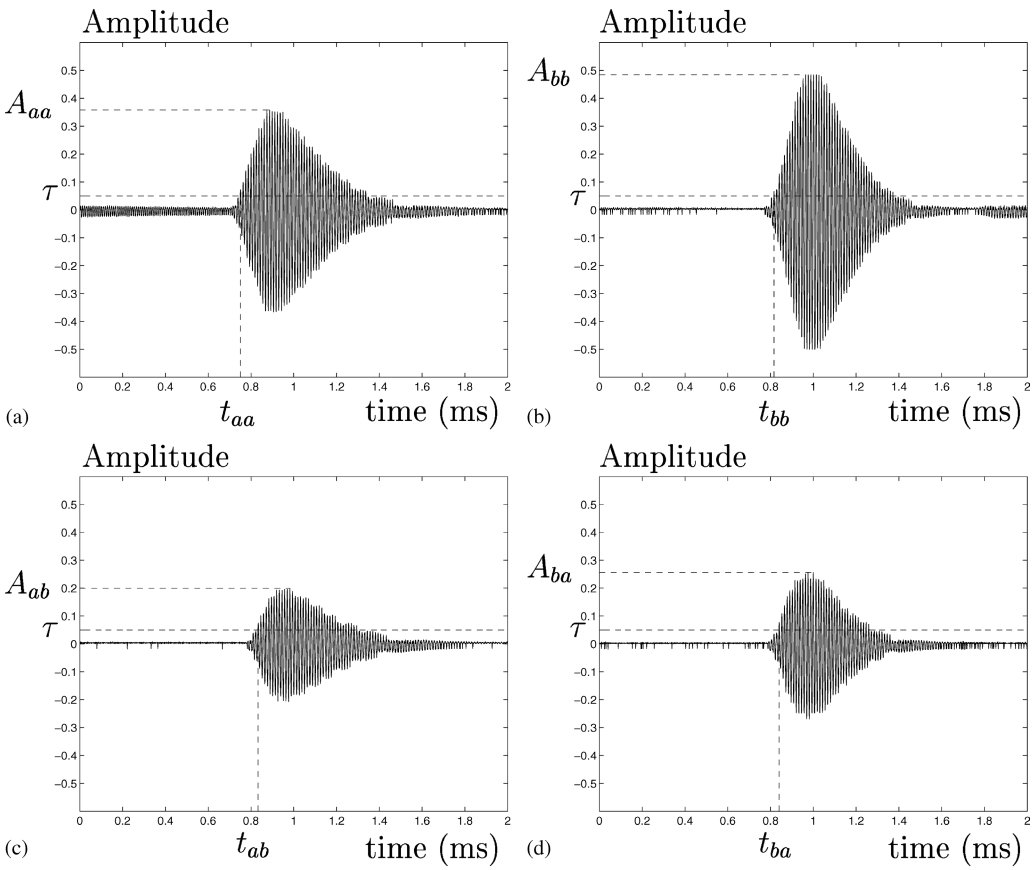

Fig. 5. Real sonar signals obtained from a planar target when (a) transducer a transmits and transducer a receives, (b) transducer b transmits and b receives, (c) transducer a transmits and b receives, (d) transducer b transmits and a receives.

Since the cross terms $A_{ab}(\alpha)$ and $A_{ba}(\alpha)$ (and $t_{ab}(\alpha)$ and $t_{ba}(\alpha)$) should ideally be equal due to reciprocity, it is more representative to employ their average. Thus, 58 samples each of the following six functions are taken collectively as acoustic signatures embodying shape and position information of a given target:

$$A_{aa}(\alpha), \quad A_{bb}(\alpha), \quad \frac{A_{ab}(\alpha)+A_{ba}(\alpha)}{2},$$
$$t_{aa}(\alpha), \quad t_{bb}(\alpha), \quad \text{and} \quad \frac{t_{ab}(\alpha)+t_{ba}(\alpha)}{2}. \tag{1}$$

We construct three alternative feature vector representations from the scans given in Eq. (1):

$$\mathbf{x}_A : \left[\mathbf{A}_{aa}, \mathbf{A}_{bb}, \frac{\mathbf{A}_{ab}+\mathbf{A}_{ba}}{2}, \mathbf{t}_{aa}, \mathbf{t}_{bb}, \frac{\mathbf{t}_{ab}+\mathbf{t}_{ba}}{2}\right]^{\mathrm{T}},$$
$$\mathbf{x}_B : [\mathbf{A}_{aa}-\mathbf{A}_{ab}, \mathbf{A}_{bb}-\mathbf{A}_{ba}, \mathbf{t}_{aa}-\mathbf{t}_{ab}, \mathbf{t}_{bb}-\mathbf{t}_{ba}]^{\mathrm{T}},$$
$$\mathbf{x}_C : [(\mathbf{A}_{aa}-\mathbf{A}_{ab})(\mathbf{A}_{bb}-\mathbf{A}_{ba}), (\mathbf{A}_{aa}-\mathbf{A}_{ab})+(\mathbf{A}_{bb}-\mathbf{A}_{ba}),$$
$$\times(\mathbf{t}_{aa}-\mathbf{t}_{ab})(\mathbf{t}_{bb}-\mathbf{t}_{ba}), (\mathbf{t}_{aa}-\mathbf{t}_{ab})+(\mathbf{t}_{bb}-\mathbf{t}_{ba})]^{\mathrm{T}}. \tag{2}$$

Here, $\mathbf{A}_{aa}$ denotes the row vector representing the samples of $A_{aa}(\alpha)$ at the 58 scan angles. The products appearing in $\mathbf{x}_C$ are componentwise products. We will evaluate the use of all three of these alternative feature vectors in the FCM clustering algorithm discussed in the next section. The first feature vector $\mathbf{x}_A$ is taken as the original form of the scans, except for averaging the cross terms ($\mathbf{A}_{ab}$ is averaged with $\mathbf{A}_{ba}$, and $\mathbf{t}_{ab}$ is averaged with $\mathbf{t}_{ba}$). The choice of the second feature vector $\mathbf{x}_B$ has been motivated by the target differentiation algorithm developed by Ayrulu and Barshan [26] and used with artificial neural network classifiers in Ref. [31]. The third feature vector $\mathbf{x}_C$ is motivated by the differential terms which are used to assign belief values to the target types in Dempster–Shafer evidential reasoning and majority voting [26]. Note that the dimensionalities d of these vector representations are 348 ($=6\times 58$) for $\mathbf{x}_A$ and 232 ($=4\times 58$) for $\mathbf{x}_B$ and $\mathbf{x}_C$.

Higher-order reflections can be of concern in sonar systems. In our system, higher-order reflections from features of the same target are already accounted for as part of the signature of that target. As for reflections from other features or targets in the environment, since we always consider the first reflection that exceeds the threshold, higher-order reflections from them are almost always irrelevant, unless the targets are very closely spaced.

3. Fuzzy *c*-means (FCM) clustering algorithm

In this section, we outline the algorithm used for clustering and differentiating the targets. We associate a class w_i with each target type ($i=1,\ldots,c$), where c is the number of classes. Each individual observation is characterized by its feature vector representation $\mathbf{x}=(x_1,\ldots,x_d)^{\mathrm{T}}$ where $\mathbf{x}$ is one of the three choices in Eq. (2).

Clustering tries to identify the relationships among patterns in a data set by organizing the patterns into a number of clusters, where the patterns in each cluster show a certain degree of closeness or similarity. In *hard clustering*, cluster boundaries are assumed to be well defined and each feature vector in the data set belongs to one of the clusters with a degree of membership equal to one. However, this type of clustering may not be suitable when the membership of each feature vector is not unambiguous. In such cases, *fuzzy clustering*, where the cluster boundaries are not well defined, is a more useful technique where each feature vector $\mathbf{x}_j$, $j=1,\ldots,N$ in the data set is assigned to each cluster i with a degree of membership $\mu_i(\mathbf{x}_j)\in[0,1]$. N is the total number of feature vectors. It is possible to use fuzzy clustering as the basis for hard clustering, by assigning feature vector $\mathbf{x}$ to cluster k (in the hard sense) if $\mu_k(\mathbf{x})\geqslant\mu_i(\mathbf{x})$, $\forall i=1,\ldots,c$ where $c\geqslant 2$ is the total number of clusters. However, it should be noted that these sets may not be disjoint when more than one maximum exists.

The FCM clustering algorithm [32,33] minimizes the following objective function with respect to fuzzy membership $\mu_{ij}\triangleq\mu_i(\mathbf{x}_j)$ and cluster centers $\mathbf{v}_i$:

$$J_m=\sum_{i=1}^{c}\sum_{j=1}^{N}\mu_{ij}^m\|\mathbf{x}_j-\mathbf{v}_i\|_{\mathbf{A}}^2,$$
$$\text{where } \|\mathbf{x}\|_{\mathbf{A}}^2=\mathbf{x}^{\mathrm{T}}\mathbf{A}\mathbf{x}. \tag{3}$$

Here, $\mathbf{A}$ is a $d\times d$ positive-definite matrix, and $1<m<\infty$ is the weighting exponent or the fuzziness index which controls the fuzziness of the resulting clusters. The set of fuzzy membership values μ_{ij} can be conveniently arrayed as a $c\times N$ matrix $\mathbf{U}\triangleq[\mu_{ij}]$. In this study, we have taken $\mathbf{A}$ as a $d\times d$ identity matrix (Euclidean norm) and $m=2$. The FCM clustering algorithm can be summarized as [33,34]:

(1) Initialize the memberships μ_{ij} such that $\sum_{i=1}^{c}\mu_{ij}=1$, $j=1,\ldots,N$.
(2) Compute the cluster center $\mathbf{v}_i$ for $i=1,\ldots,c$ using

$$\mathbf{v}_i=\frac{\sum_{j=1}^{N}\mu_{ij}^m\mathbf{x}_j}{\sum_{j=1}^{N}\mu_{ij}^m}. \tag{4}$$

(3) Update the memberships μ_{ij} for $i=1,\ldots,c$ and $j=1,\ldots,N$ using

$$\mu_{ij}=\frac{(\|\mathbf{x}_j-\mathbf{v}_i\|_{\mathbf{A}}^2)^{-1/(m-1)}}{\sum_{k=1}^{c}(\|\mathbf{x}_j-\mathbf{v}_k\|_{\mathbf{A}}^2)^{-1/(m-1)}} \tag{5}$$

(4) Repeat the second and third steps until the value of J_m in Eq. (3) no longer decreases. This completes the fuzzy clustering. To determine the class to which each feature vector $\mathbf{x}_j$ belongs, we simply find the class for which μ_{ij} is maximum.

The fuzzy c-means algorithm always converges to strict local minima of J_m, starting from an initial guess of μ_{ij}, though different choices of initial μ_{ij} might lead to different local minima [33,34].

The above procedure determines the cluster centers and membership values for a given value of c, and does not involve the determination of the value of c which corresponds to the number of different kinds of targets. In order to find this value of c, a cluster validity criterion is applied. A fuzzy validity criterion for fuzzy clustering algorithms has been proposed in Ref. [34]. Among a number of other validity criteria, this criterion has been shown to be the most reliable and to provide the best results over a wide range of choices for the number of clusters (2–10), and for m from 1.01 to 7 [35]. This validity criterion depends on the data set, the distance between cluster centers, and the fuzzy membership values computed by the above procedure and has the following functional definition:

$$S \triangleq \frac{\sum_{i=1}^{c}\sum_{j=1}^{N}\mu_{ij}^2\|\mathbf{x}_j-\mathbf{v}_i\|^2}{N\min_{i,j\ (i\neq j)}\|\mathbf{v}_i-\mathbf{v}_j\|^2}. \tag{6}$$

Here, $\|\cdot\|$ is the usual Euclidean norm. This criterion balances the compactness and the separation of the clusters. In this equation, the term

$$\pi \triangleq \frac{\sum_{i=1}^{c}\sum_{j=1}^{N}\mu_{ij}^2\|\mathbf{x}_j-\mathbf{v}_i\|^2}{N} \tag{7}$$

is defined as the *compactness* of the fuzzy c-partition of the data set, which is the ratio of the *total variation* of the data set with respect to the fuzzy c-partition, to the total number of patterns in the data set (and is thus the average variation of the data set). A smaller π corresponds to a fuzzy c-partition with more compact clusters. The term $s \triangleq \min_{i,j\ (i\neq j)}\|\mathbf{v}_i-\mathbf{v}_j\|^2$ is defined as the *separation* of a fuzzy c-partition where a larger s indicates larger separation between the clusters. Since $S=\pi/s$, a smaller S indicates a partition in which all the clusters are compact and separate from each other.

The overall procedure can be summarized as follows: First, we find the $\mathbf{v}_i$ and μ_{ij} corresponding to each value of c by using the four-step FCM clustering algorithm outlined above. Then, by using the $\mathbf{v}_i$ and μ_{ij} values obtained with this algorithm, we calculate the validity criterion S for each c and pick the value of c yielding the smallest value of S. This gives us the number of different types of targets in the environment. Then, the hard membership of any $\mathbf{x}_j$ can be determined by choosing the class corresponding to the maximum value of μ_{ij}.

4. Position estimation

The range r and azimuth θ can be estimated from TOF information using triangulation. Given the TOF measurements t_{aa} and t_{bb}, we can write the following expressions for the range and azimuth of the target:

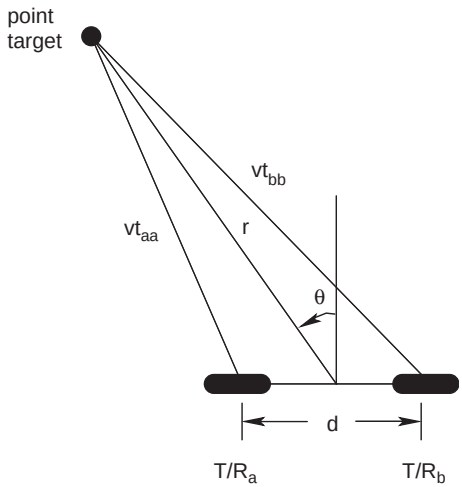

Fig. 6. Point target geometry.

$$r=\sqrt{\frac{\frac{v^2}{2}(t_{aa}^2+t_{bb}^2)-d^2}{4}}, \tag{8}$$

$$\theta=\sin^{-1}\left(\frac{v^2(t_{bb}^2-t_{aa}^2)}{4d\sqrt{\frac{v^2}{2}(t_{aa}^2+t_{bb}^2)-d^2}}\right), \tag{9}$$

where d is the separation of the transducers and v is the speed of sound in air. These expressions have been derived for a point target using simple geometry (Fig. 6). In our case, where a whole series of TOF measurements are available as a function of α, averaging over the values of r and θ calculated for each value of α will result in a more reliable estimate. While this approach provides reasonable estimates in the absence of knowledge regarding the target universe and the lack of target-specific models, the resulting accuracy may not always be satisfactory since the reflection characteristics of specific targets such as planes, corners, and so forth differ significantly from that of a point target.

Much higher accuracy can be obtained by employing model-based formulas for estimating r and θ. Detailed reflection models for this purpose have been derived in Ref. [26]. The results presented in Ref. [26] can be reworked into a form compatible with this paper (see Appendix A) and are presented below ($t'_{ab} \triangleq (t_{ab}+t_{ba})/2$).

Plane:

$$r=\frac{v(t_{aa}+t_{bb})}{4}, \tag{10}$$

$$\theta=\sin^{-1}\left(\frac{v(t_{bb}-t_{aa})}{2d}\right). \tag{11}$$

Corner:

$$r = \frac{vt'_{ab}}{2}, \tag{12}$$

$$\theta = \sin^{-1}\left(\frac{v(t_{bb}^2 - t_{aa}^2)}{4dt'_{ab}}\right). \tag{13}$$

Edge:

$$r = \sqrt{\frac{\frac{v^2}{2}(t_{aa}^2 + t_{bb}^2) - d^2}{4}}, \tag{14}$$

$$\theta = \sin^{-1}\left(\frac{v^2(t_{bb}^2 - t_{aa}^2)}{4d\sqrt{\frac{v^2}{2}(t_{aa}^2 + t_{bb}^2) - d^2}}\right). \tag{15}$$

Cylinder:

$$r \cong \frac{\sqrt{v^2 t'^2_{ab} - d^2}}{2}, \tag{16}$$

$$\theta \cong \sin^{-1}\left(\frac{\frac{v^2}{4}(t_{aa}^2 - t_{bb}^2) + y[v(t_{aa} - t_{bb}) - 2d]}{d\sqrt{v^2 t'^2_{ab} - d^2}}\right), \tag{17}$$

where

$$y \triangleq \frac{\frac{v^2 t'^2_{ab}}{2} - \frac{v^2}{4}(t_{aa}^2 + t_{bb}^2)}{v(t_{aa} + t_{bb}) - 2\sqrt{v^2 t'^2_{ab} - d^2}}. \tag{18}$$

Acute corner:

$$\theta = \sin^{-1}\left(\frac{(t_{bb}^2 - t_{aa}^2)(2r^2 + \frac{d^2}{2})}{2dr(t_{bb}^2 + t_{aa}^2)}\right). \tag{19}$$

Although an explicit formula for r cannot be written for the acute corner, r can be estimated by solving a quadratic equation whose coefficients are presented in Appendix A.

In the event that it is desired to use such target-specific formulas, it is necessary to know and analyze beforehand the objects which might be encountered, and identify each class with a particular target model. A straightforward approach is to obtain beforehand a reference set of feature vectors corresponding to each target in the universe, situated in the center of the field of view of the sensing system, and then find the target whose reference vector is at a minimum distance to a particular cluster center (not the individual feature vectors). This approach has been employed to estimate the ranges and azimuths of the targets in our experiments and calculate the mean errors.

5. Experimental results

Details of the experimental configuration were presented in Section 2 and are not repeated here. The experiments were conducted in a closed room without any major drafts or acoustic noise. The data were collected at different times of the day and night without regard to time-varying environmental conditions such as noise, temperature, pressure, etc. No special effort was made to isolate noise or control the temperature or pressure. The targets have been clustered by using the FCM clustering algorithm for $2 \leqslant c \leqslant 10$, using each of the three feature vector representations defined in Eq. (2). Then, the value of the validity criterion S defined in Eq. (6) has been calculated for each representation and each value of c. These values are plotted in Fig. 7. We observe that the minimum value of S is obtained when $c = 7$ in all three cases, corresponding to the actual number of different targets in our experiments. When $c = 2$, planes, edges, and cylinders with all three radii are included in one cluster and corners and acute corners are classified in another cluster for all three data sets. When $c = 3$, planes are separated from edges and cylinders into a new cluster. When the number of clusters is increased to 4, edges are classified into a new cluster. Acute corners are distinguished from corners when c is further incremented by one. When $c = 6$, cylinders with $r_c = 2.5$ cm are moved to a new cluster. Finally, cylinders with $r_c = 5.0$ cm are separated from cylinders with $r_c = 7.5$ cm when $c = 7$. Further increasing the number of clusters results in artificial fragmentation of the feature vectors into two or three clusters. For example, planes located along the line-of-sight of the transducer are included in one cluster and the remaining planes are collected into another cluster, or the planes to the left and right of the line-of-sight are further split into two different clusters.

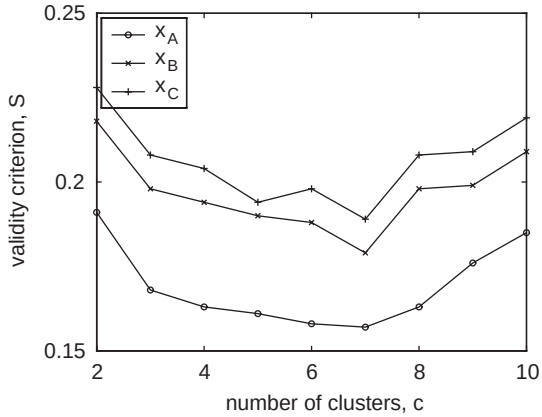

Fig. 7. Values of the validity criterion S versus the number of clusters c for the feature vector representations $\mathbf{x}_A, \mathbf{x}_B$, and $\mathbf{x}_C$.

Correct target differentiation rates of 98%, 93%, and 93% are achieved using the feature vector representations $\mathbf{x}_A, \mathbf{x}_B$, and $\mathbf{x}_C$, respectively; the feature vector representation $\mathbf{x}_A$ results in the highest percentage of correct classification among the three alternatives. The mean range and azimuth errors found by averaging the absolute values of the errors over all targets in our data set are 0.5 cm in range and 0.8° in azimuth. The greatest contribution to these errors comes from targets which are incorrectly differentiated, since in

this case incorrect range and azimuth estimation formulas are employed. However, since a high 98% correct differentiation is achieved, this does not have a significant impact.

The conditions under which the experimental data were obtained differ from typical application scenarios where the observation platform and/or the targets may be in motion. Results obtained from the experiments will be representative of such application scenarios under the following assumptions:

(1) the relative motion of the observation platform and targets is not too fast,
(2) the targets are not too densely situated so that two or more targets are not simultaneously in the joint sensitivity region.

While these assumptions would be satisfied under a wide range of circumstances, removing them would require considerably more sophisticated modeling.

6. Conclusion

In this paper, the fuzzy c-means clustering algorithm is used in conjunction with a cluster validity criterion which balances compactness and separation, to determine the number of different types of targets in an environment, based on their sonar signatures. The information extracted from these signatures consists of the amplitude and the TOF values of the sonar echoes. Based on this information, the class of each target and its location are also determined. The fact that the targets are located at different positions with respect to the observer complicates the classification problem, since identical or similar targets must be grouped in the same class despite the fact that their sonar signatures are altered as a result of their different positions. The method is experimentally verified using real sonar returns from targets in indoor environments. Three alternative feature vector representations have been compared and the one resulting in the best differentiation accuracy is determined. We have considered amplitude and TOF data in their raw and differential form. The representation corresponding to the raw amplitude and TOF values gave the highest correct differentiation rate of 98%. The mean of the absolute values of range and azimuth errors were 0.5 cm and 0.8°, respectively.

The demonstrated approach can find a variety of applications in situations where an intelligent system, such as a robot, encounters several different types of targets at different positions in its environment. Future work involves testing our system in a scenario where a mobile robot tries to identify the targets in its environment for simultaneous map building and localization. One of the issues which would have to be addressed to this end is ensuring that the degree of relative motion of the robot and the targets is not so fast as to violate the conditions necessary for proper operation (see the end of Section 5) and how to recognize and handle occasional violations of these conditions. Another issue is to study the robustness of the system to larger amounts of noise and clutter. It would also be interesting to investigate how the system works with more loosely defined target types, such as human beings crudely modeled as cylinders. The present system can deal with minor to moderate perturbations from the ideal target types without much difficulty, but clustering objects exhibiting greater variations is a more challenging problem. Finally, of great interest would be to consider the fusion of sonar information with information from other sensing modalities, in particular optical sensors.

Acknowledgements

This research was supported by TÜBİTAK under grants 197E051, EEEAG-116, and EEEAG-92.

Appendix A

Here we show how the results of Ref. [26] can be modified for the purposes of this paper. In Ref. [26], r_a and r_b denote the distances corresponding to the TOF measurements when the same transducer transmits and receives its own signal. Although t_{ab} and t_{ba} are ideally equal, their measured values will not be identical due to noise and measurement errors. Therefore, their average $t'_{ab} \triangleq (t_{ab} + t_{ba})/2$ is employed.

Plane:

For the planar target, the range r and azimuth θ are given by Eqs. (10) and (11) of Ref. [26] as follows:

$$r = \frac{r_a + r_b}{2}, \tag{20}$$

$$\theta = \sin^{-1}\left(\frac{r_b - r_a}{d}\right). \tag{21}$$

Substituting $r_a = vt_{aa}/2$ and $r_b = vt_{bb}/2$, we get

$$r = \frac{v(t_{aa} + t_{bb})}{4}, \tag{22}$$

$$\theta = \sin^{-1}\left(\frac{v(t_{bb} - t_{aa})}{2d}\right). \tag{23}$$

Corner:

For the corner target, the range r and azimuth θ are given by Eqs. (70) and (13) of Ref. [26] as

$$t_{ab} = t_{ba} = \frac{2r}{v}, \tag{24}$$

$$\theta = \sin^{-1}\left(\frac{r_b^2 - r_a^2}{2dr}\right). \tag{25}$$

Writing $t_{ab} + t_{ba} = 4r/v$, using the definition of t'_{ab}, and extracting r, we obtain

$$r = \frac{vt'_{ab}}{2}. \tag{26}$$

Substituting $r_a = vt_{aa}/2$ and $r_b = vt_{bb}/2$ in Eq. (25), we get θ as follows:

$$\theta = \sin^{-1}\left(\frac{v(t_{bb}^2 - t_{aa}^2)}{4dt'_{ab}}\right). \tag{27}$$

Edge:

For the edge, the range r and azimuth θ are given by Eqs. (12) and (13) of Ref. [26]:

$$r = \sqrt{\frac{r_a^2 + r_b^2 - \frac{d^2}{2}}{2}}, \tag{28}$$

$$\theta = \sin^{-1}\left(\frac{r_b^2 - r_a^2}{2dr}\right). \tag{29}$$

Substituting $r_a = vt_{aa}/2$ and $r_b = vt_{bb}/2$, we get

$$r = \sqrt{\frac{\frac{v^2}{2}(t_{aa}^2 + t_{bb}^2) - d^2}{4}}, \tag{30}$$

$$\theta = \sin^{-1}\left(\frac{v^2(t_{bb}^2 - t_{aa}^2)}{4d\sqrt{\frac{v^2}{2}(t_{aa}^2 + t_{bb}^2) - d^2}}\right). \tag{31}$$

Cylinder:

In Ref. [26], Eqs. (14)–(16) for the cylinder are given as

$$r \cong \frac{\sqrt{(r_1 + r_2)^2 - d^2}}{2}, \tag{32}$$

$$\theta \cong \sin^{-1}\left[\frac{(r_a^2 - r_b^2) + 2y(r_a - r_b - d)}{2\sqrt{(r_1 + r_2)^2 - d^2}}\right], \tag{33}$$

$$y \cong \frac{\frac{(r_1+r_2)^2}{2} - (r_a^2 + r_b^2)}{2(r_b + r_a - \sqrt{(r_1 + r_2)^2 - d^2})}, \tag{34}$$

where $r_1 + r_2$ is the distance-of-flight corresponding to the TOF value when one transducer transmits and the other receives. Substituting $r_a = vt_{aa}/2$, $r_b = vt_{bb}/2$, and $(r_1 + r_2)^2 = v^2 t'^2_{ab}$ in the above equations, we get

$$r \cong \frac{\sqrt{v^2 t'^2_{ab} - d^2}}{2}, \tag{35}$$

$$\theta \cong \sin^{-1}\left(\frac{\frac{v^2}{4}(t_{aa}^2 - t_{bb}^2) + y[v(t_{aa} - t_{bb}) - 2d]}{d\sqrt{v^2 t'^2_{ab} - d^2}}\right), \tag{36}$$

where

$$y \triangleq \frac{\frac{v^2 t'^2_{ab}}{2} - \frac{v^2}{4}(t_{aa}^2 + t_{bb}^2)}{v(t_{aa} + t_{bb}) - 2\sqrt{v^2 t'^2_{ab} - d^2}}. \tag{37}$$

Acute corner:

Referring to Eq. (3) in Ref. [26] for the angular position of the acute corner:

$$\theta = \sin^{-1}\left[\frac{(r_{bb}^2 - r_{aa}^2)(2r^2 + \frac{d^2}{2})}{2dr(r_{bb}^2 + r_{aa}^2)}\right], \tag{38}$$

where r_{aa} and r_{bb} are the distance-of-flight values corresponding to the TOF values t_{aa} and t_{bb}, respectively. Substituting $r_{aa} = vt_{aa}$ and $r_{bb} = vt_{bb}$, we get

$$\theta = \sin^{-1}\left(\frac{(t_{bb}^2 - t_{aa}^2)(2r^2 + \frac{d^2}{2})}{2dr(t_{bb}^2 + t_{aa}^2)}\right). \tag{39}$$

Although an explicit formula for r cannot be written for the acute corner, r can be estimated by solving the following equation (Eq. (6) in Ref. [26]):

$$Ax^2 + Bx + C = 0, \quad \text{where}$$

$$x = 2r^2 + \frac{d^2}{2}. \tag{40}$$

In Eqs. (7)–(9) of Ref. [26], the coefficients of this polynomial are given as

$$A = \left(\frac{r_{aa}^2 - r_{bb}^2}{r_{bb}^2}\right)^2, \tag{41}$$

$$B = \left(\frac{r_{aa}^2 + r_{bb}^2}{r_{bb}^2}\right)\left\{r_{aa}^2 - \frac{1}{r_{bb}^2}[(r_{aa}^2 + r_{bb}^2) \times (r_{ab}^2 + d^2) - (r_{ab}^2 - d^2)^2]\right\}, \tag{42}$$

$$C = d^2 r_{ab}^2 \left(\frac{r_{aa}^2 + r_{bb}^2}{r_{bb}^2}\right)^2, \tag{43}$$

where r_{ab} is the distance-of-flight value corresponding to the TOF value t_{ab}. Substituting $r_{aa} = vt_{aa}$, $r_{bb} = vt_{bb}$, and $r_{ab} = vt'_{ab}$, we get

$$A = \left(\frac{t_{aa}^2 - t_{bb}^2}{t_{bb}^2}\right)^2, \tag{44}$$

$$B = \left(\frac{t_{aa}^2 + t_{bb}^2}{t_{bb}^2}\right)\left(v^2 t_{aa}^2 - \frac{1}{v^2 t_{bb}^2}[v^2(t_{aa}^2 + t_{bb}^2) \times (v^2 t'^2_{ab} + d^2) - (v^2 t'^2_{ab} - d^2)^2]\right), \tag{45}$$

$$C = d^2 v^2 t'^2_{ab}\left(\frac{t_{aa}^2 + t_{bb}^2}{t_{bb}^2}\right)^2. \tag{46}$$

References

[1] R. Kuc, M.W. Siegel, Physically-based simulation model for acoustic sensor robot navigation, IEEE Trans. Pattern Anal. Machine Intell. PAMI-9 (1987) 766–778.

[2] R. Kuc, B.V. Viard, A physically-based navigation strategy for sonar-guided vehicles, Int. J. Robotics Res. 10 (1991) 75–87.

[3] R. Kuc, B. Barshan, Navigating vehicles through an unstructured environment with sonar, in: Proceedings of IEEE International Conference on Robotics and Automation, Scottsdale, AZ, 14–19 May 1989, pp. 1422–1426.

[4] A. Elfes, Sonar based real-world mapping and navigation, IEEE Trans. Robotics Automation RA-3 (1987) 249–265.

[5] J.J. Leonard, H.F. Durrant-Whyte, Directed Sonar Navigation, Kluwer Academic Press, London, UK, 1992.

[6] O. Bozma, R. Kuc, A physical model-based analysis of heterogeneous environments using sonar—ENDURA method, IEEE Trans. Pattern Anal. Machine Intell. 16 (1994) 497–506.

[7] A. Kurz, Constructing maps for mobile robot navigation based on ultrasonic range data, IEEE Trans. Systems, Man, Cybernet. B: Cybernet. 26 (1996) 233–242.

[8] R. Kuc, Three-dimensional tracking using qualitative bionic sonar, Robotics Autonomous Systems 11 (2) (1993) 213–219.

[9] J. Borenstein, Y. Koren, Obstacle avoidance with ultrasonic sensors, IEEE Trans. Robotics Automation RA-4 (1988) 213–218.

[10] H. Peremans, K. Audenaert, J.M. Van Campenhout, A high-resolution sensor based on tri-aural perception, IEEE Trans. Robotics Automation 9 (1993) 36–48.

[11] L. Kleeman, R. Kuc, Mobile robot sonar for target localization and classification, Int. J. Robotics Res. 14 (1995) 295–318.

[12] F.T.S. Yu, S. Jutamulia (Ed.), Optical Pattern Recognition, Cambridge University Press, Cambridge, 1998.

[13] F.T.S. Yu, S. Yin (Ed.), Selected Papers on Optical Pattern Recognition, Vol. MS 156 of SPIE Milestone Series, Bellingham, SPIE Optical Engineering Press, Washington, 1999.

[14] D. Casasent, D. Psaltis, Scale invariant optical correlation using Mellin transforms, Opt. Comm. 17 (1976) 59–63.

[15] F.T.S. Yu, X. Li, E. Tam, S. Jutamulia, D.A. Gregory, Rotation invariant pattern recognition with a programmable joint transform correlator, Appl. Opt. 28 (1989) 4725–4727.

[16] C. Gu, J. Hong, S. Campbell, 2-D shift invariant volume holographic correlator, Opt. Comm. 88 (1992) 309–314.

[17] Polaroid Corporation, Ultrasonic Components Group, 119 Windsor St., Polaroid Manual, Cambridge, MA, 1997.

[18] B. Barshan, B. Ayrulu, Performance comparison of four time-of-flight estimation methods for sonar signals, Electron. Lett. 34 (1998) 1616–1617.

[19] O. Bozma, R. Kuc, Building a sonar map in a specular environment using a single mobile sensor, IEEE Trans. Pattern Anal. Machine Intell. 13 (1991) 1260–1269.

[20] O. Bozma, R. Kuc, Characterizing pulses reflected from rough surfaces using ultrasound, J. Acoustical Soc. Am. 89 (1991) 2519–2531.

[21] A.M. Sabatini, Statistical estimation algorithms for ultrasonic detection of surface features, in: Proceedings of the IEEE/RSJ International Conference on Intelligent Robots and Systems, Munich, Germany, 12–16 September 1994, pp. 1845–1852.

[22] B. Barshan, A.Ş. Sekmen, Radius of curvature estimation and localization of targets using multiple sonar sensors, J. Acoustical Soc. Am. 105 (1999) 2318–2331.

[23] M.L. Hong, L. Kleeman, Ultrasonic classification and location of 3-D room features using maximum likelihood estimation I, Robotica 15 (1997) 483–491.

[24] M.L. Hong, L. Kleeman, Ultrasonic classification and location of 3-D room features using maximum likelihood estimation II, Robotica 15 (1997) 645–652.

[25] J. Manyika, H.F. Durrant-Whyte, Data Fusion and Sensor Management: A Decentralized Information-Theoretic Approach, Ellis Horwood, New York, 1994.

[26] B. Ayrulu, B. Barshan, Identification of target primitives with multiple decision-making sonars using evidential reasoning, Int. J. Robotics Res. 17 (1998) 598–623.

[27] B. Barshan, R. Kuc, Differentiating sonar reflections from corners and planes by employing an intelligent sensor, IEEE Trans. Pattern Anal. Machine Intell. 12 (1990) 560–569.

[28] R. Kuc, Biomimetic sonar recognizes objects using binaural information, J. Acoustical Soc. Am. 102 (1997) 689–696.

[29] Panasonic Corporation, Ultrasonic ceramic microphones, 12 Blanchard Road, Burlington, MA, 1989.

[30] B. Ayrulu, B. Barshan, Reliability measure assignment to sonar for robust target differentiation, Pattern Recognition 35 (2002) 1403–1419.

[31] B. Barshan, B. Ayrulu, S.W. Utete, Neural network-based target differentiation using sonar for robotics applications, IEEE Trans. Robotics Automation 16 (2000) 435–442.

[32] J.C. Dunn, A fuzzy relative of the ISODATA process and its use in detecting compact well-separated clusters, J. Cybernetics 3 (1974) 32–57.

[33] J.C. Bezdek, Pattern Recognition with Fuzzy Objective Function Algorithms, Plenum, New York, 1981, p. 80.

[34] X.L. Xie, G. Beni, A validity measure for fuzzy clustering, IEEE Trans. Pattern Anal. Machine Intell. PAMI-13 (1991) 841–847.

[35] N.R. Pal, J.C. Bezdek, On cluster validity for the fuzzy *c*-means model, IEEE Trans. Fuzzy Systems 3 (1995) 370–379.

About the Author—BILLUR BARSHAN received B.S. degrees in both electrical engineering and in physics from Boğaziçi University, Istanbul, Turkey and the M.S. and Ph.D. degrees in electrical engineering from Yale University, New Haven, Connecticut, in 1986, 1988, and 1991, respectively. Dr. Barshan was a research assistant at Yale University from 1987 to 1991, and a postdoctoral researcher at the Robotics Research Group at University of Oxford, U.K. from 1991 to 1993. She joined Bilkent University, Ankara in 1993 where she is currently a professor at the Department of Electrical Engineering. Dr. Barshan is the founder of the Robotics and Sensing Laboratory in the same department. She is the recipient of the 1994 Nakamura Prize awarded to the most outstanding paper in 1993 IEEE/RSJ Intelligent Robots and Systems International Conference, 1998 TÜBİTAK Young Investigator Award, and 1999 Mustafa N. Parlar Foundation

Research Award. Dr. Barshan's current research interests include intelligent sensors, sonar and inertial navigation systems, sensor-based robotics, and multi-sensor data fusion.

About the Author—BIRSEL AYRULU received the B.S. degree in electrical engineering from Middle East Technical University and the M.S. and Ph.D. degrees in electrical engineering from Bilkent University, Ankara, Turkey in 1994, 1996, and 2001 respectively. Her current research interests include intelligent sensing, sonar sensing, sensor data fusion, learning methods, target differentiation, and sensor-based robotics.